The Effect of Temperature on the London Dispersive and Lewis Acid-base Surface Energies of Poly Methyl Methacrylate Adsorbed on Silica by Inverse Gas Chromatography

Tayssir Hamieh *

Posted Date: 23 April 2024

doi: 10.20944/preprints202404.1469.v1

Keywords: Hamieh thermal effect; London dispersive surface energy; polar surface energy; recovery fraction; transition temperatures

Article

The Effect of Temperature on the London Dispersive and Lewis Acid-base Surface Energies of Poly Methyl Methacrylate Adsorbed on Silica by Inverse Gas Chromatography

Tayssir Hamieh [1,2]

[1] Faculty of Science and Engineering, Maastricht University, P.O. Box 616, 6200 MD Maastricht, The Netherlands; t.hamieh@maastrichtuniversity.nl

[2] Laboratory of Materials, Catalysis, Environment and Analytical Methods (MCEMA), Faculty of Sciences, Lebanese University, Hadath, Beirut, P.O. Box 6573/14, Lebanon

Abstract: Inverse gas chromatography at infinite dilution was used to determine the surface thermodynamic properties of silica particles and PMMA adsorbed on silica, and more particularly, to quantify the London dispersive energy γ_s^d, the Lewis acid γ_s^+ and base γ_s^- polar surface energies of PMMA/silica composites as a function of the temperature and the recovery fraction θ of PMMA. The polar acid–base surface energy γ_s^{AB} and the total surface energy of the different composites were then deduced as a function of the temperature. In this paper, the Hamieh thermal model was used to quantify the surface thermodynamic energy of poly methyl methacrylate (PMMA) adsorbed on silica particles at different recovery fractions. A comparison of the new results was carried out with those obtained by applying other molecular models of the surface areas of organic molecules adsorbed on the different solid substrates. An important deviation of these molecular models from the thermal model was proved. The determination of γ_s^d, γ_s^+, γ_s^-, and γ_s^{AB} of PMMA in both bulk and adsorbed phases showed an important non-linearity variation of these surface parameters as a function of the temperature. The presence of maxima in the curves of $\gamma_s^d(T)$ highlighted the second order transition temperatures in PMMA showing beta-relaxation, glass transition and liquid-liquid temperatures. These three transition temperatures depended on the adsorption rate of PMMA on silica. The proposed method gave a new relation between the recovery fraction of PMMA and its London dispersive energy showing an important effect of the temperature on the surface energy parameters of adsorption of PMMA on silica. A universal equation relating $\gamma_s^d(T,\theta)$ of the systems PMMA/silica to the recovery fraction and the temperature was proposed.

Keywords: Hamieh thermal effect; London dispersive surface energy; polar surface energy; recovery fraction; transition temperatures

1. Introduction

The estimation of the London dispersive and acid-base surface energies of solids, oxides and polymers [1–14] is of crucial importance in many industrial processes such as, adhesion, paints, coatings, corrosion, chemical reactions, adsorption, and catalysis. The most used technique to determine these surface parameters was the inverse gas chromatography (IGC) at infinite dilution. The net retention time and volume of organic solvents adsorbed on solid surfaces, experimentally obtained by IGC, are directly correlated to the surface thermodynamic properties of solid materials, such as the London dispersive $\gamma_s^d(T)$ and polar $\gamma_s^p(T)$ components of the surface energy of solid particles as a function of the temperature. The interesting IGC technique used to characterize the surface and polar characteristics of materials was applied more particularly for determining the London dispersive energy of ligno-cellulosic fibers [15] based on works of Jacob et al. [16], Carvalho et al. [17], Chtourou et al. [18], Dorris and Gray [19], Donnet et al. [20] and Gutmann [21].

Gamble et al. [22] determined the surface energy characteristics of drug substance coated with two grades of silicon dioxide was studied by IGC using the Dorris and Gray approach. IGC technique

 doi:10.20944/preprints202404.1469.v1

was used by Balard et al. [23] to determine the surface properties of milled graphites, by Bogillo et al. [24] to evaluate the surface free energy components for heterogeneous solids, and by Das et al. [25,26] to study the surface energy distributions of lactose and pharmaceutical powders. The Adsorption of n-alkanes at zero surface coverage on cellulose paper and wood fibres [27] and solid surface polarity [27] using IGC at infinite dilution. Feeley et al. [29] studied the surface properties and flow characteristics of salbutamol sulphate; and the surface energy characteristics of micronized materials were determined [30]. The same technique was also used to measure the surface energy and high energy sites for mixtures of crystalline and amorphous lactose [31,32]. Kołodziejek et al. [33] studied the relationship between surface properties determined by inverse gas chromatography and ibuprofen release from hybrid materials based on fumed silica. Whereas, Ho et al. [34–36] studied by IGC the surface energy heterogeneity of crystals. Many authors studied the surface energies of some polymers as tosylate functionalized poly(ethylene glycol) [37], polybutadiene/fillers [38], poly(2,2,3,3,3-pentafluoropropyl methacrylate) [39], hyperbranched poly(ester amide) [40].

In this paper, we used The IGC technique [35–67] at infinite dilution to determine the dispersive $\gamma_s^d(T)$ and polar $\gamma_s^p(T)$ components of the surface energy of poly (methyl methacrylate) (PMMA) adsorbed on silica at different recovery fractions as a function of the temperature by using our new approach based on the Hamieh thermal model [41–43] that gave the variations of the surface area of adsorbed organic molecules as a function of the temperature.

2. IGC Methods and Materials

The experimental values of the net retention time t_n and volume V_n of the adsorbed organic solvents on PMMA and silica were obtained from the direct measurements by using inverse gas chromatography (IGC) at infinite dilution [41–67]. The London dispersive energy was determined by using the concept of Fowkes based on the geometric mean of the respective values of the London dispersive components of the surface energy of the non-polar molecule γ_l^d and the solid substrate γ_s^d. The non-polar solvents generally used in IGC technique were the n-alkanes (from n-pentane C5 to n-decane C10). The determination of $RTlnV_n$ of n-alkanes adsorbed on PMMA/silica at different temperatures will lead to the values of $\gamma_s^d(T)$ by using the following relation:

$$RTlnV_n = 2\mathcal{N}a\left(\gamma_l^d\gamma_s^d\right)^{1/2} + \alpha(T) \quad (1)$$

where T is the absolute temperature of the chromatographic column containing the solid material, R the perfect gas constant, a the surface area of an adsorbed molecule, $\mathcal{N}$ is the Avogadro number, and $\alpha(T)$ is a constant depending only on the temperature and the solid material.

Relation 1 was used to deduce the value of γ_s^d by supposing both γ_l^d and a parameters as constant. Hamieh criticized the above approximation in several studies [41–43,62–67] by proving an important thermal effect on the surface area of organic molecules adsorbed on the solid surfaces. We previously proposed different molecular models allowing the determination of the surface areas of molecules [55], by using Kiselev results, the two-dimensional Van der Waals (VDW) and Redlich–Kwong (R-K) equations, the geometric, cylindrical, and spherical model. However, the most accurate model was that based on the thermal model [41–43] that gave the expressions of the surface area $a(T)$ of organic molecules as a function of the temperature, and those of $\gamma_l^d(T)$ relative to the different molecules.

A commercial Focus GC gas chromatograph apparatus equipped with a flame ionization detector (FID) was used in this study to obtain the net retention time and volume of different n-alkanes that were injected into a stainless-steel column (with a 2 mm inner diameter and a length of 20 cm) containing the solid particles. The temperature range varied from 30 °C to 200 °C. The same experimental procedure as that used in other studies [64–68] was applied on PMMA/silica. The used n-alkanes (pentane, hexane, heptane, octane, nonane) of highly pure grade (99%) were purchased from local chemical society.

The flow rate of the carrier gas (helium) was 20 mL/min, whereas, the temperatures of the injector and detector were fixed at 200 °C. The infinite dilution of the probes was realized with the help of 1 µL-Hamilton syringes, by injecting very small quantities of the vapor solvent, satisfying the

 doi:10.20944/preprints202404.1469.v1

limit of detection of the FID of high sensitivity, to practically realize the zero-surface coverage [67]. All columns containing PMMA and silica particles were preconditioned at 130 °C overnight to remove any adsorbed water molecules or other residual impurities.

PMMA and silica solid particles with different recovery fractions of PMMA (varying from 0 to 1.0) used in this work were the same solid materials previously characterized in other studies using other chromatographic methods [55,68].

3. Experimental Results

3.1. London Dispersive Surface Energy of Silica particles

The values of $RTlnV_n$ and $2\mathcal{N}a\left(\gamma_l^d\right)^{1/2}$ of silica particles at different temperatures were given in Tables S1 and S2 by taking into account the thermal effect of the temperature on the surface area of organic solvents. Figure 1 gave the variations of $\gamma_s^d\ (T)$ of silica as a function of the temperature using Hamieh thermal model.

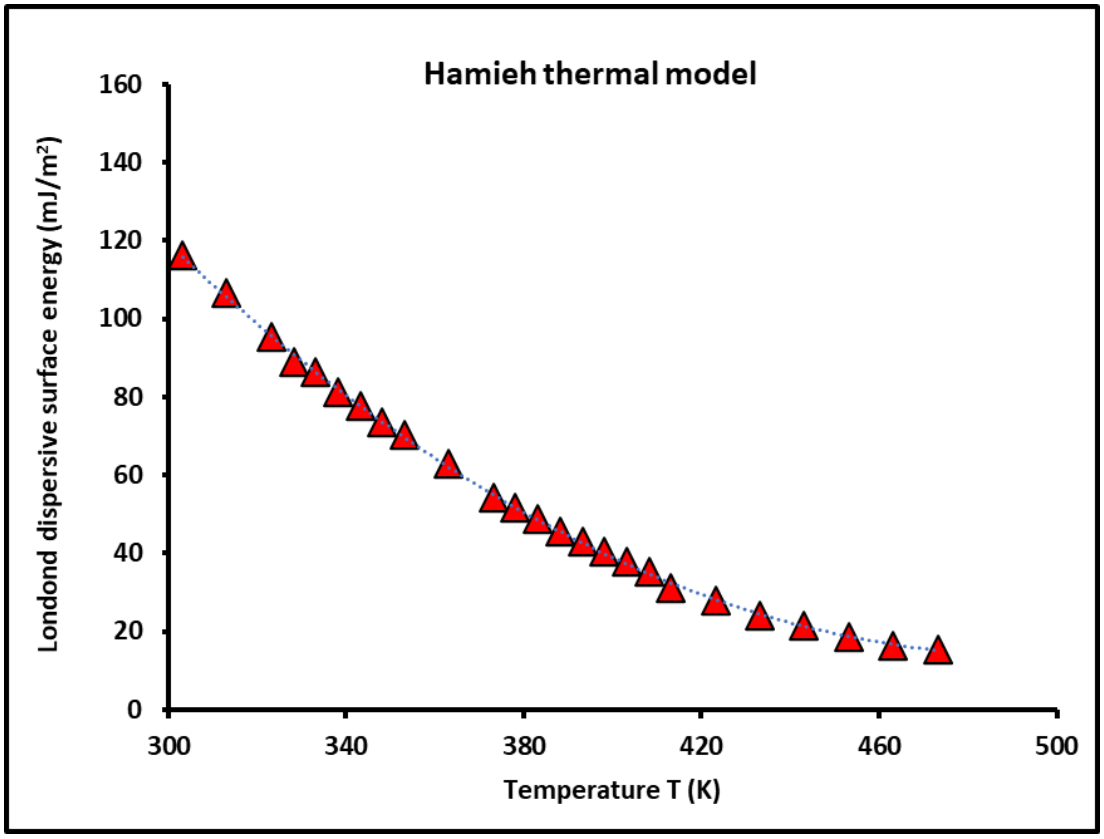

Figure 1. Evolution of $\gamma_s^d\ (T)$ of silica particles as a function of the temperature using Hamieh thermal model.

Figure 1 showed that the monotonous decrease of the London dispersive surface energy of silica is not perfectly linear. The non-linear variation of $\gamma_s^d\ (T)$ can be approached by parabolic interpolation in this case. Equation (2) was obtained with an excellent regression coefficient (R^2 = 0.9994) in the studied domain of temperature:

$$\gamma_s^d(T) = 2.8 \times 10^{-3}T^2 - 2.76T + 691.29 \quad (2)$$

The comparison of this result with that obtained by using other molecular models can be shown in Figure 2.

 doi:10.20944/preprints202404.1469.v1

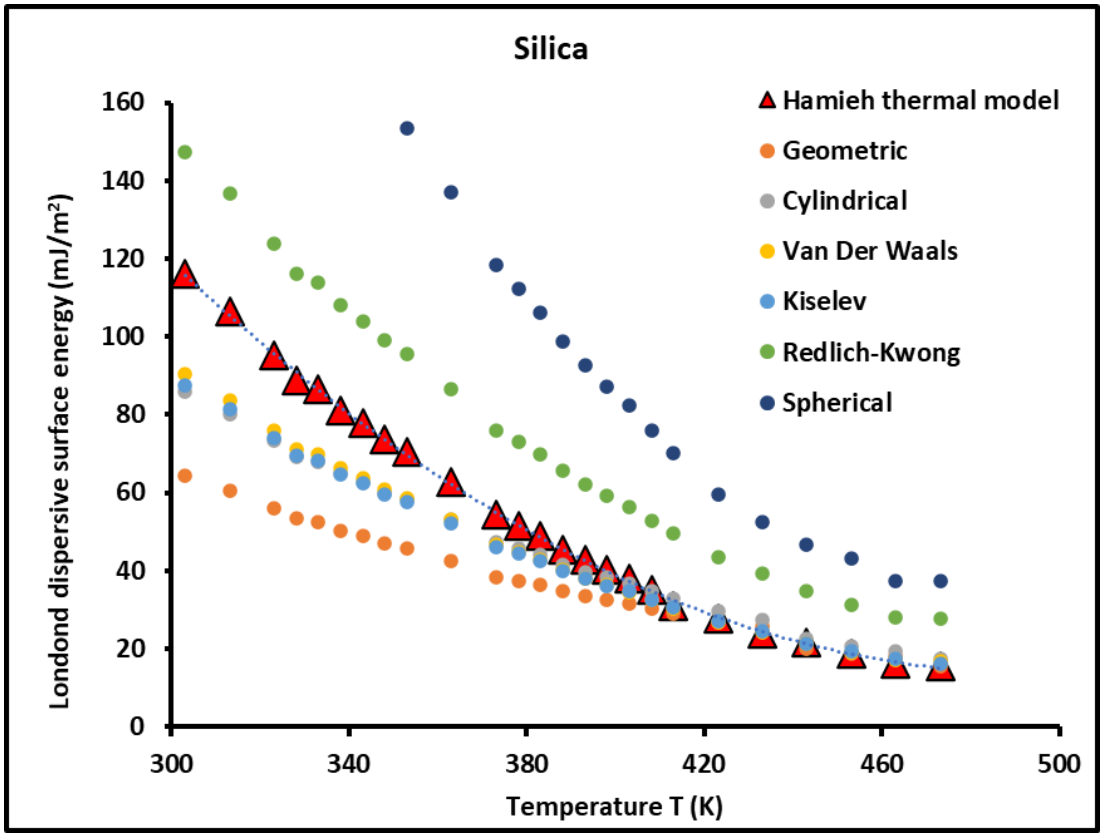

Figure 2. Variations of $\gamma_s^d\ (T)$ of silica particles as a function of the temperature using the various models compared to Hamieh thermal model.

The results presented in Figure 2 and Table 1 showed the monotonous variations of $\gamma_s^d\ (T)$ of silica particles for all used molecular models with parabolic curves. However, an important deviation of all models was observed with the respect of Hamieh thermal model. Indeed, the spherical model overestimated the values of the London dispersive surface energy of solid materials, whereas, the geometric model underestimated the values of $\gamma_s^d\ (T)$, while the cylindrical, Kiselev and Van der Waals models are the closest to that of the thermal model.

Table 1. Values of $\gamma_s^d\ (T)\ (in\ mJ/m^2)$ of silica particles as a function of the temperature using the various models and the new Hamieh thermal model

T(K)	Hamieh thermal model	Geometric	Cylindrical	Van Der Waals	Kiselev	Redlich-Kwong	Spherical
303.15	116.29	64.36	85.89	90.32	87.55	147.35	253.33
313.15	106.48	60.64	80.22	83.74	81.35	136.6	232.09
323.15	95.37	55.98	73.36	75.97	73.97	123.92	207.92
328.15	88.87	53.59	69.12	71.26	69.48	116.24	193.73
333.15	86.42	52.4	67.96	69.78	68.13	113.83	188.45
338.15	81.23	50.33	64.91	66.22	64.86	108.02	177.77

 doi:10.20944/preprints202404.1469.v1

343.15	77.81	48.84	62.64	63.73	62.39	103.95	169.66
348.15	73.68	47.11	60.05	60.79	59.6	99.16	160.63
353.15	70.45	45.91	58.16	58.57	57.51	95.54	153.56
363.15	62.86	42.65	53.3	53.1	52.31	86.61	136.95
373.15	54.33	38.5	47.41	46.68	46.14	76.13	118.24
378.15	51.68	37.5	45.8	44.8	44.37	73.06	112.41
383.15	48.93	36.39	44.05	42.8	42.48	69.8	106.33
388.15	45.55	34.78	41.72	40.22	40.01	65.6	98.87
393.15	43.01	33.48	39.78	38.08	37.96	62.11	92.62
398.15	40.28	32.5	38.22	36.29	36.27	59.19	87.27
403.15	38.02	31.63	36.78	34.62	34.69	56.47	82.25
408.15	35.25	30.3	34.81	32.47	32.62	52.95	76.13
413.15	31.13	29.07	32.93	30.41	30.64	49.59	70.32
423.15	27.85	26.93	29.55	26.65	27.04	43.46	59.71
433.15	23.93	25.9	27.45	24.21	24.7	39.48	52.37
443.15	21.53	19.93	22.67	21.38	21.41	34.88	46.62
453.15	18.74	18.79	20.75	19.11	19.26	31.17	43.1
463.15	16.34	18.13	19.28	17.23	17.49	28.11	37.52
473.15	15.47	15.65	17.5	16.96	16.16	27.66	37.41

This large deviation (Table 1) resulted from the fact that the effect of the temperature on the surface area of molecules was neglected in the above models. Only the results of the thermal model can be considered as accurate. The closest results to those of the thermal model was obtained by Van der Waals model.

3.2. Study of $\gamma_s^d(T)$ of PMMA and PMMA/Silica Composites

Figure 3 brings together the results of the London dispersive surface energy of PMMA particles obtained by the various applied molecular models compared to those of the thermal model. It can be observed that the results of the molecular models extremely deviate from those of Hamieh thermal model. However, the general tendency of all drawn curves in Figure 3 and shown in Table 2 highlighted the same values of the three maxima of temperatures. These three maxima showed the presence of three transition temperatures that were proved in other studies [55,68]. The beta-

 doi:10.20944/preprints202404.1469.v1

relaxation temperature, the glass transition and the liquid-liquid temperatures were respectively obtained at 60°C, 110°C, and 160°C, located on the different maxima of $\gamma_s^d(T)$ as shown in Figure 3 and in Table 2 (in bold dark red). The curves obtained by the thermal model and those of cylindrical, Kiselev, geometric, and Van de Waals models are mixed up after a temperature of 400K.

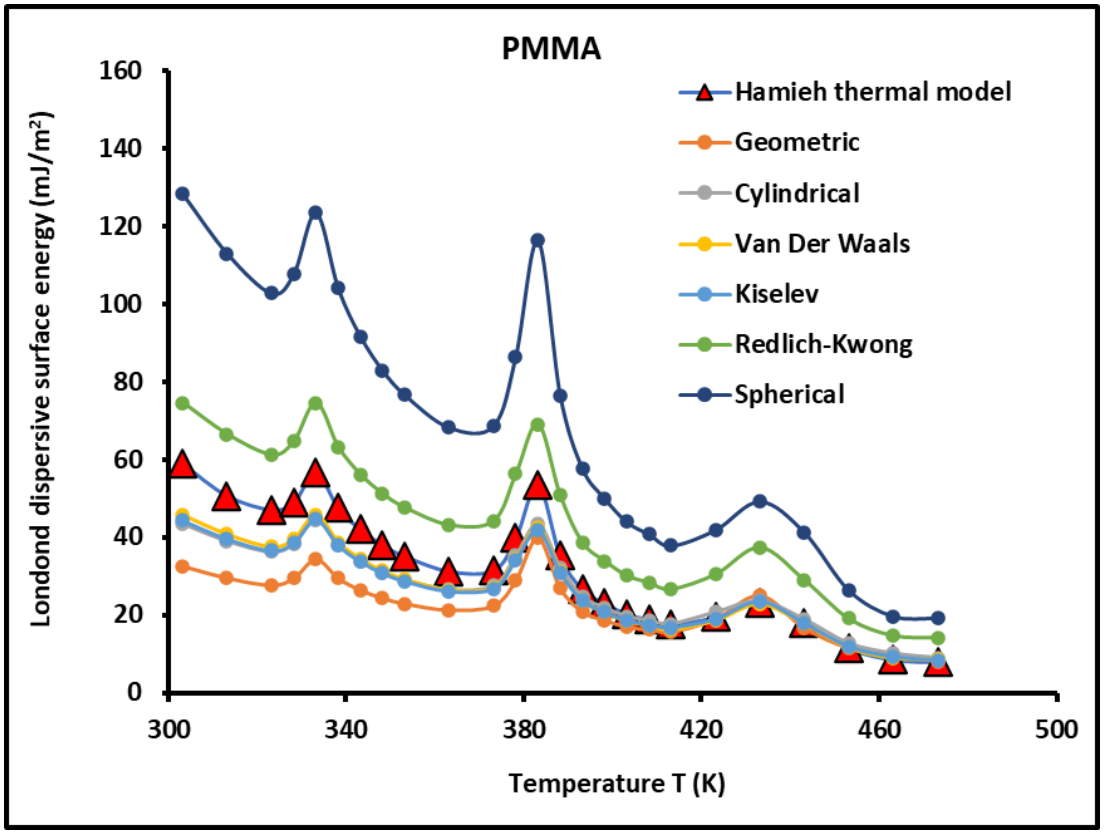

Figure 3. Variations of $\gamma_s^d(T)$ of PMMA in bulk phase as a function of the temperature using the various molecular models.

Table 2. Values of $\gamma_s^d(T)\ (in\ mJ/m^2)$ of PMMA as a function of the temperature using the different models.

T(K)	Hamieh thermal model	Geometric	Cylindrical	Van Der Waals	Kiselev	Redlich-Kwong	Spherical
303.15	58.87	32.58	43.48	45.73	44.32	74.61	128.26
313.15	50.68	29.5	39.03	40.75	39.58	66.47	112.94
323.15	47.11	27.65	36.23	37.53	36.54	61.23	102.73
328.15	49.08	29.49	38.44	39.65	38.66	64.69	107.82
333.15	**56.62**	**34.33**	**44.52**	**45.72**	**44.63**	**74.58**	**123.47**
338.15	47.53	29.45	37.98	38.76	37.96	63.22	104.05
343.15	42.03	26.38	33.83	34.43	33.7	56.16	91.65

 doi:10.20944/preprints202404.1469.v1

348.15	38.03	24.31	30.99	31.38	30.76	51.19	82.93
353.15	35.14	22.89	29	29.22	28.68	47.66	76.6
363.15	31.31	21.23	26.54	26.45	26.05	43.14	68.21
373.15	31.53	22.34	27.51	27.09	26.78	44.18	68.63
378.15	39.80	28.87	35.26	34.49	34.17	56.26	86.57
383.15	**53.54**	**39.82**	**43.41**	**42.36**	**41.9**	**69.1**	**116.35**
388.15	35.24	26.89	32.26	31.12	30.95	50.75	76.52
393.15	26.59	20.85	24.77	23.72	23.64	38.68	57.69
398.15	23.08	18.62	21.89	20.79	20.78	33.91	50.01
403.15	20.31	16.9	19.65	18.51	18.53	30.18	43.96
408.15	18.87	16.22	18.63	17.38	17.46	28.35	40.77
413.15	17.54	15.63	17.71	16.35	16.74	26.67	37.83
423.15	19.53	18.88	20.72	18.69	18.96	30.48	41.87
433.15	**23.16**	**25.01**	**23.62**	**22.91**	**23.47**	**37.37**	**49.22**
443.15	17.91	16.58	18.85	17.79	17.81	29.01	41.27
453.15	11.48	11.5	12.71	11.71	11.79	19.1	26.4
463.15	8.58	9.51	10.12	9.05	9.18	14.76	19.71
473.15	7.93	8.04	8.98	8.68	8.29	14.16	19.16

The highest non-linearity of the curves $\gamma_s^d\ (T)$ of PMMA was observed in all molecular models in the temperature interval [300K; 500K]. This non-linearity is certainly due to the presence of transition phenomena in PMMA submitted to the surface group changes when the temperature increases. All molecular models are largely deviated from the thermal model. The deviation reached 300% in many cases. However, the results obtained by those models can be considered as qualitative, whereas, the thermal model gave the most accurate results.

The results relative to the adsorption of PMMA on silica particles were presented in Figure 4 and Table 3 at different recovery fractions varying from $\theta = 0$ (case of pure silica particles) to $\theta = 1.0$ (representing a monolayer of PMMA on silica). The results in Figure 4 and Table 3 clearly showed the large difference in the values the London dispersive surface energy of the composites PMMA/silica when the temperature and the recovery fraction changed. Three interesting results were detected:

Preprints.org (www.preprints.org) | NOT PEER-REVIEWED | Posted: 23 April 2024 doi:10.20944/preprints202404.1469.v1

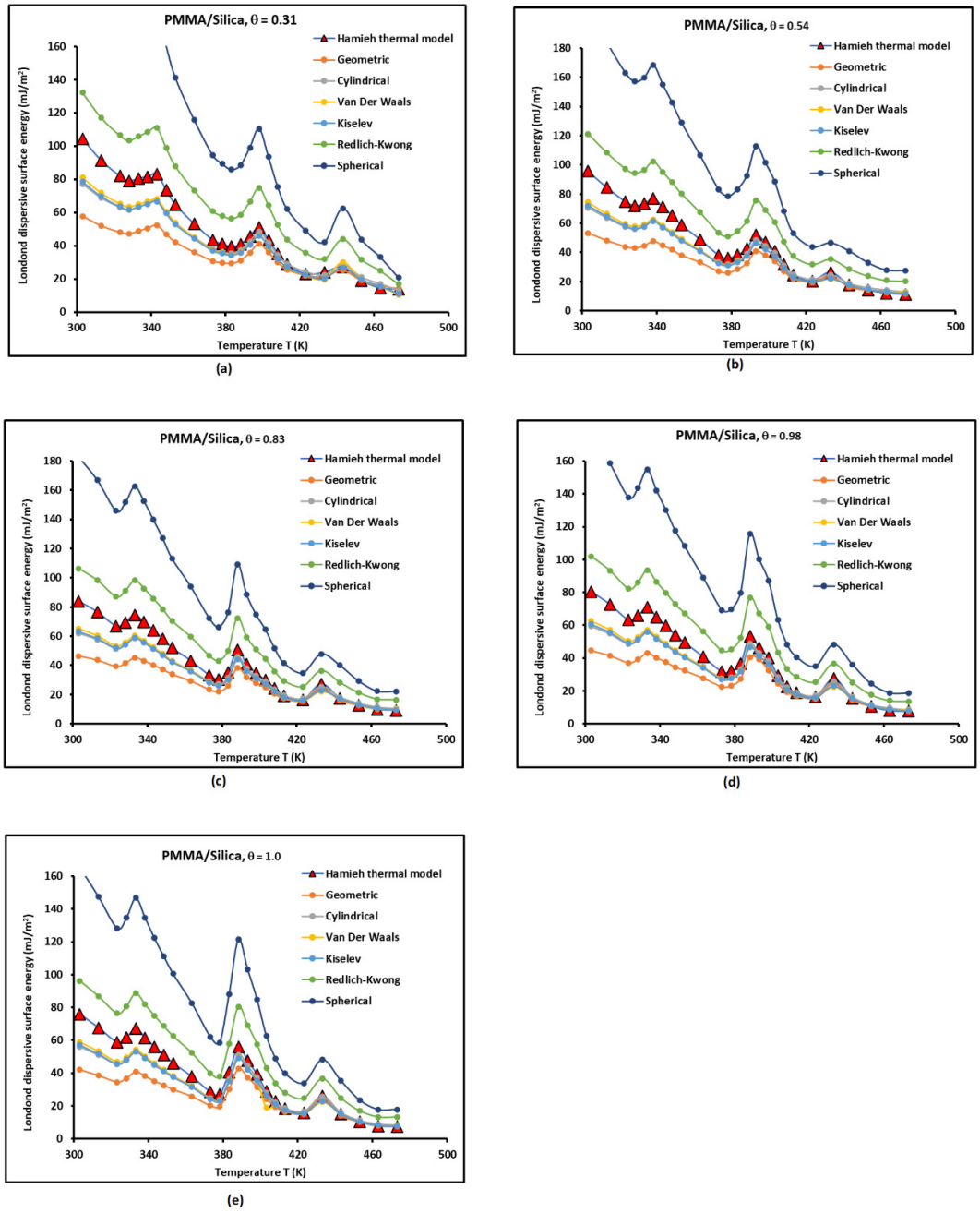

Figure 4. Variations of $\gamma_s^d\ (T)$ of PMMA adsorbed on silica particles as a function of the temperature, at different recovery fractions from $\theta = 0.31$ to $\theta = 1.0$, using the various molecular models: (a) $\theta = 0.31$, (b) $\theta = 0.54$, (c) $\theta = 0.83$, (d) $\theta = 0.98$, and (e) $\theta = 1.0$.

Table 3. Values of $\gamma_s^d\ (T)$ of PMMA adsorbed on silica particles as a function of the temperature, at different recovery fractions from $\theta = 0.31$ to $\theta = 1.0$, using the various molecular models. N.B.: the bold dark red figures are relative to the transition temperatures.

Adsorption of PMMA on silica for $\theta = 0.31$							
T(K)	**Hamieh thermal model**	**Geometric**	**Cylindrical**	**Van Der Waals**	**Kiselev**	**Redlich-Kwong**	**Spherical**
303.15	104.37	57.76	77.09	81.07	78.57	132.24	227.37
313.15	91.30	51.99	68.78	71.80	69.75	117.13	199.00

 doi:10.20944/preprints202404.1469.v1

323.15	81.98	48.12	63.06	65.31	63.59	106.54	178.75
328.15	78.95	47.09	61.39	63.31	61.73	103.28	172.15
333.15	80.44	48.78	63.26	64.95	63.41	105.95	175.41
338.15	81.52	50.51	65.15	66.46	65.09	108.41	178.40
343.15	**83.10**	**52.17**	**66.90**	**68.05**	**66.63**	**111.01**	**181.19**
348.15	73.51	47.00	59.91	60.65	59.46	98.93	160.25
353.15	64.73	42.18	53.43	53.82	52.84	87.78	141.09
363.15	53.21	36.09	45.11	44.94	44.27	73.31	115.91
373.15	43.45	30.79	37.91	37.33	36.90	60.88	94.56
378.15	41.08	29.80	36.40	35.60	35.27	58.07	89.35
383.15	39.48	29.35	35.54	34.53	34.27	56.33	85.81
388.15	40.75	31.10	37.30	35.98	35.79	58.69	88.48
393.15	45.69	35.85	42.56	40.74	40.62	66.45	99.10
398.15	**50.97**	**41.15**	**48.37**	**46.28**	**45.89**	**74.90**	**110.42**
403.15	43.24	36.00	41.84	39.38	39.46	64.23	93.55
408.15	35.25	30.10	34.52	32.17	32.33	52.47	75.41
413.15	28.80	25.66	29.07	26.84	27.04	43.78	62.08
423.15	22.94	22.18	24.34	21.95	22.27	35.80	49.18
433.15	23.99	21.38	22.44	19.60	20.07	31.96	42.09
443.15	**27.13**	**25.13**	**28.57**	**29.95**	**26.99**	**43.95**	**62.52**
453.15	19.05	19.10	21.09	19.42	19.57	31.68	43.80
463.15	14.48	16.06	17.08	15.27	15.50	24.91	33.25
473.15	13.85	14.04	13.03	10.36	11.03	16.89	20.69

Adsorption of PMMA on silica for $\theta = 0.54$

T(K)	Hamieh thermal model	Geometric	Cylindrical	Van Der Waals	Kiselev	Redlich-Kwong	Spherical
303.15	95.71	53.22	70.69	74.34	72.05	121.26	208.47
313.15	84.53	48.13	63.67	66.47	64.57	108.43	184.23
323.15	74.85	43.93	57.57	59.62	58.06	97.26	163.19
328.15	72.05	42.97	56.03	57.78	56.34	94.26	157.12
333.15	73.29	44.44	57.63	59.17	57.77	96.53	159.81
338.15	**76.92**	**47.65**	**61.43**	**62.71**	**61.42**	**102.29**	**168.35**
343.15	71.19	44.68	57.31	58.31	57.08	95.12	155.23
348.15	65.49	41.87	53.37	54.03	52.97	88.14	142.77
353.15	58.91	38.09	48.43	49.22	48.08	80.29	129.15
363.15	48.96	33.21	41.51	41.36	40.74	67.46	106.65
373.15	38.16	27.04	33.3	32.78	32.41	53.47	83.06
378.15	36.12	26.2	32	31.31	31.01	51.06	78.57
383.15	38.33	28.5	34.51	33.53	33.28	54.69	83.32
388.15	42.68	32.58	39.08	37.7	37.5	61.49	92.7
393.15	**52.06**	**40.83**	**48.5**	**46.42**	**46.28**	**75.72**	**112.92**
398.15	46.88	37.86	44.5	42.24	42.22	68.89	101.55
403.15	40.96	34.09	39.63	37.3	37.37	60.84	88.61
408.15	31.95	27.28	31.29	29.16	29.31	47.56	68.36
413.15	24.69	22.04	24.95	23.01	23.19	37.52	53.18
423.15	20.39	19.71	21.63	19.51	19.79	31.82	43.71
433.15	**26.55**	**23.63**	**24.79**	**21.66**	**22.18**	**35.31**	**46.51**
443.15	17.74	16.42	18.67	17.61	17.64	28.73	40.87
453.15	14.20	14.35	15.85	14.61	14.71	23.82	32.94
463.15	12.12	13.44	14.29	12.78	12.97	20.84	27.82

 doi:10.20944/preprints202404.1469.v1

473.15	11.41	11.57	12.92	12.85	11.93	20.38	27.57
Adsorption of PMMA on silica for $\theta = 0.83$							
T(K)	**Hamieh thermal model**	**Geometric**	**Cylindrical**	**Van Der Waals**	**Kiselev**	**Redlich-Kwong**	**Spherical**
303.15	83.96	46.46	62.01	65.21	63.21	106.39	182.9
313.15	76.57	43.6	57.67	60.22	58.49	98.23	166.91
323.15	66.94	39.29	51.49	53.33	51.93	87	145.96
328.15	69.57	41.49	54.1	55.79	54.4	91.02	151.71
333.15	**74.62**	**45.24**	**58.68**	**60.25**	**58.82**	**98.29**	**162.72**
338.15	69.65	43.16	55.67	56.79	55.62	92.64	152.46
343.15	64.16	40.28	51.65	52.55	51.44	85.72	139.91
348.15	58.34	37.3	47.55	48.14	47.19	78.53	127.2
353.15	52.02	33.95	42.98	43.21	42.47	70.48	113.27
363.15	43.21	29.31	36.63	36.5	35.96	59.54	94.14
373.15	33.20	23.52	28.97	28.52	28.19	46.52	72.26
378.15	30.44	22.08	26.97	26.38	26.13	43.04	66.22
383.15	35.11	26.1	31.61	30.71	30.48	50.09	76.31
388.15	**50.63**	**38.41**	**46.07**	**44.44**	**44.2**	**72.48**	**109.28**
393.15	40.82	32.01	38.03	36.4	36.29	59.37	88.54
398.15	34.59	27.92	32.83	31.17	31.15	50.84	74.96
403.15	29.88	24.86	28.9	27.21	27.26	44.38	64.64
408.15	24.15	20.61	23.64	22.04	22.15	35.94	51.66
413.15	19.32	17.21	19.5	18.01	18.14	29.37	41.65
423.15	16.27	15.72	17.26	15.57	15.8	25.39	34.89
433.15	27.30	24.3	25.49	22.26	22.8	36.31	47.82
443.15	**17.37**	**16.08**	**18.28**	**17.25**	**17.27**	**28.14**	**40.03**
453.15	12.73	12.76	14.1	12.99	13.08	21.19	29.29
463.15	9.74	10.79	11.48	10.27	10.42	16.75	22.36
473.15	9.17	9.30	10.39	10.04	9.59	16.38	22.16
Adsorption of PMMA on silica for $\theta = 0.98$							
T(K)	**Hamieh thermal model**	**Geometric**	**Cylindrical**	**Van Der Waals**	**Kiselev**	**Redlich-Kwong**	**Spherical**
303.15	80.49	44.54	59.44	62.52	60.6	101.99	175.35
313.15	72.76	41.43	54.81	57.22	55.58	93.35	158.6
323.15	63.27	37.13	48.66	50.4	49.07	82.22	137.94
328.15	65.85	39.28	51.21	52.81	51.49	86.15	143.6
333.15	**70.99**	**43.04**	**55.83**	**57.32**	**55.96**	**93.51**	**154.82**
338.15	64.89	40.21	51.86	52.91	51.82	86.31	142.04
343.15	59.74	37.5	48.09	48.93	47.9	79.81	130.25
348.15	54.14	34.5	44.12	44.68	43.79	72.87	117.65
353.15	49.63	32.34	40.97	41.27	40.52	67.32	108.2
363.15	40.84	27.7	34.62	34.5	33.98	56.27	88.97
373.15	31.81	22.54	27.76	27.33	27.02	44.58	69.25
378.15	32.08	23.19	28.37	27.82	27.54	45.38	69.63
383.15	36.69	27.28	33.04	32.1	31.86	52.36	79.76
388.15	**53.25**	**40.64**	**48.75**	**47.02**	**46.77**	**76.68**	**115.61**
393.15	46.15	39.19	43.00	41.16	41.03	67.13	100.11
398.15	40.22	32.46	38.16	36.24	36.21	59.1	87.13
403.15	29.26	24.35	28.31	26.65	26.7	43.47	63.32
408.15	22.52	19.22	22.05	20.55	20.66	33.52	48.18
413.15	18.87	16.79	19.04	17.59	17.72	28.7	40.63

 doi:10.20944/preprints202404.1469.v1

423.15	16.30	15.75	17.29	15.6	15.82	25.44	34.96
433.15	27.59	24.55	25.75	22.49	23.04	36.68	48.31
443.15	**15.59**	**14.42**	**16.41**	**15.48**	**15.5**	**25.25**	**35.92**
453.15	10.59	10.61	11.72	10.8	10.88	17.62	24.36
463.15	8.16	9.04	9.62	8.6	8.73	14.03	18.74
473.15	7.66	7.77	8.68	8.39	8.01	13.68	18.51

Adsorption of PMMA on silica for $\theta = 1.0$

T(K)	Hamieh thermal model	Geometric	Cylindrical	Van Der Waals	Kiselev	Redlich-Kwong	Spherical
303.15	75.92	42.01	56.07	58.97	57.16	96.2	165.4
313.15	67.65	38.52	50.96	53.21	51.68	86.8	147.47
323.15	58.85	34.54	45.27	46.89	45.65	76.4	128.33
328.15	61.70	36.8	47.98	49.48	48.24	80.71	134.54
333.15	**67.28**	**40.79**	**52.91**	**54.33**	**53.04**	**88.62**	**146.73**
338.15	61.50	38.11	49.15	50.15	49.12	81.8	134.63
343.15	56.07	35.19	45.14	45.93	44.96	74.92	122.27
348.15	50.99	32.6	41.56	42.08	41.25	68.64	111.18
353.15	46.12	30.05	38.07	38.35	37.65	62.55	100.54
363.15	37.96	25.75	32.18	32.07	31.59	52.31	82.71
373.15	28.47	20.17	24.84	24.46	24.18	39.9	61.97
378.15	26.94	19.54	23.87	23.36	23.13	38.09	58.61
383.15	40.51	30.1	36.45	35.41	35.15	57.76	87.99
388.15	**55.89**	**42.66**	**51.17**	**49.35**	**49.09**	**80.5**	**121.36**
393.15	47.51	37.26	44.26	42.37	42.24	69.1	103.05
398.15	39.16	31.61	37.16	35.29	35.26	57.55	84.85
403.15	28.98	24.11	28.03	18.92	26.44	43.04	62.69
408.15	22.77	19.43	22.29	20.78	20.88	33.88	48.71
413.15	18.42	16.41	18.59	17.17	17.3	28	39.71
423.15	15.79	15.26	16.75	15.11	15.33	24.65	33.87
433.15	**25.97**	**24.38**	**25.61**	**22.38**	**22.93**	**36.5**	**48.15**
443.15	15.28	14.14	16.09	15.18	15.2	24.76	35.23
453.15	10.19	10.21	11.28	10.4	10.47	16.96	23.44
463.15	7.71	8.58	9.11	8.13	8.26	13.26	17.7
473.15	7.39	7.49	8.37	8.09	7.72	13.19	17.85

- The London dispersive surface energy decreases when the recovery fraction fractions of PMMA adsorbed on silica increases whatever the used molecular model
- The adsorption of PMMA on silica strongly affects the physicochemical properties of PMMA relatively to its bulk phase. The transitions temperatures observed in PMMA alone change with the recovery fraction.
- When approaching the monolayer of adsorption of PMMA on silica particles, there is a spontaneous decreasing evolution of the London dispersive surface energy from silica particles (Table 1) to PMMA in bulk phase (Table 2) and passing through the different recovery fractions from $\theta = 0.31$ to $\theta = 1.0$ (Table 3 and Figure 4) the behavior of PMMA monolayer becomes closer to PMMA in its bulk phase.

The results given in Figure 4 and Table 3 gave the various transition temperatures of PMMA adsorbed on silica particles at different recovery fractions. The obtained values were presented in Table 4 and Figure 5. It was observed that the beta-relaxation temperature linearly decreased from $T_\beta = 343.15K$ to stabilize at $T_\beta = 333.15K$ for $\theta = 0.83$, and the same value was observed for PMMA alone. Whereas, the glass transition decreased from $T_g = 398.15K$ to $T_g = 383.15K$ for $\theta = 0.83$, and then it increased to $T_g = 388.15K$ to reach the value $T_g = 383.15K$ for PMMA. However,

Preprints.org (www.preprints.org) | NOT PEER-REVIEWED | Posted: 23 April 2024 doi:10.20944/preprints202404.1469.v1

the liquid-liquid transition temperature oscillated between $T_{l-l} = 443.15K$ and $T_{l-l} = 433.15K$. therefore, there is an important effect of the adsorption of PMMA on the London dispersive energy of the systems PMMA/silica, and on the transition temperatures. Those results were confirmed for all molecular models.

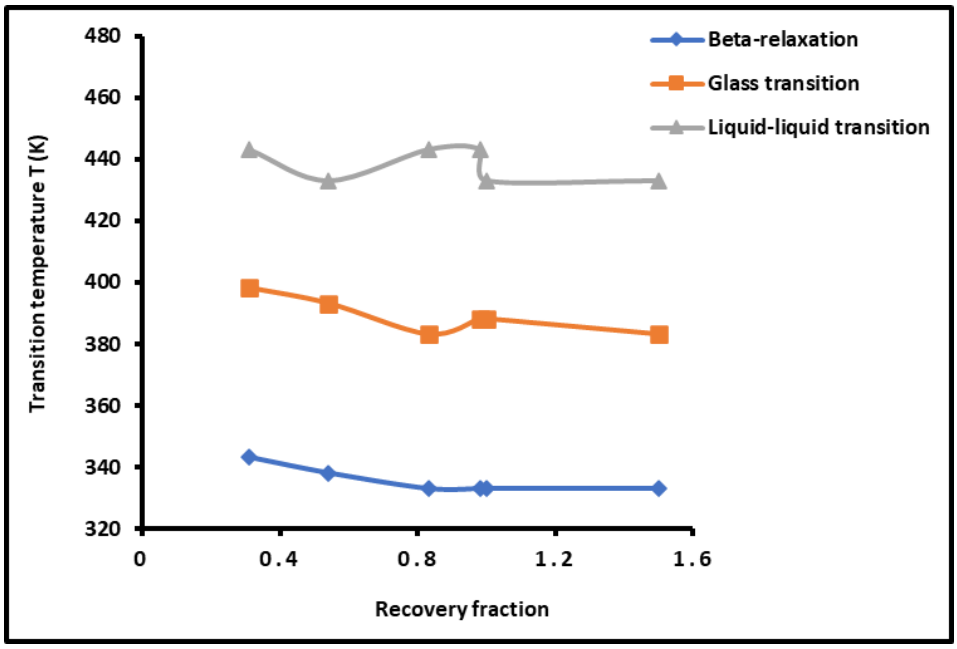

Figure 5. Evolution of the transition temperatures of PMMA adsorbed on silica particles as a function of the recovery fraction PMMA/Silica.

Table 4. Values of the transition temperatures of PMMA adsorbed on silica particles at different recovery fractions.

Recovery fraction of PMMA/silica θ	Beta-relaxation temperature $T_\beta\ (in\ K)$	Glass transition temperature $T_g\ (in\ K)$	Liquid-liquid temperature $T_{l-l}\ (in\ K)$
0.31	333.15	383.15	433.15
0.54	343.15	398.15	443.15
0.83	338.15	393.15	433.15
0.98	333.15	383.15	443.15
1.0	333.15	383.15	443.15
PMMA	333.15	388.15	433.15

Furthermore, The London dispersive surface energy of the composites PMMA/silica at the different transition temperatures strongly varied as a function of the recovery fraction. These variations of γ_s^d are clearly shown in Table 5. A decrease of the London dispersive energy was observed before reaching the monolayer in the cases of beta-relaxation and liquid-liquid transitions, whereas, a small change was found in the case of the glass transition. Table 5 also showed after the monolayer, the different values of γ_s^d approached those of PMMA.

Table 5. Values of the London dispersive surface energy $\gamma_s^d\ (mJ/m^2)$ of PMMA/silica composites at the transition temperatures as a function of the recovery fraction.

Recovery fraction of PMMA/silica θ	Beta-relaxation temperature $T_\beta\ (in\ K)$	Glass transition temperature $T_g\ (in\ K)$	Liquid-liquid temperature $T_{l-l}\ (in\ K)$

 doi:10.20944/preprints202404.1469.v1

0.31	83.10	50.97	27.13
0.54	76.92	52.06	26.55
0.83	74.62	50.63	17.37
0.98	70.99	53.26	15.59
1.0	67.28	55.89	25.97
PMMA	56.62	53.54	23.16

In fact, the above observations can be generalized for all temperatures and recovery fractions as shown in Figure 6. The curves plotted on Figure 6a showed the shift of the maxima of the various transition temperatures when the recovery fraction of PMMA/silica varied. Furthermore, the variations of $\gamma_s^d(\theta)$ were perfectly linear for all temperatures far from the transition temperatures as shown in Figure 6b. the results showed the decrease of the London dispersive surface energy of PMMA/silica when the temperature and/or the recovery increased. The different equations of $\gamma_s^d(\theta)$ were given in Table 6. The linearity was shown by the good linear regression coefficients shown in Table 6.

Table 6. Equation of London dispersive surface energy $\gamma_s^d(\theta)$ of composites PMMA/silica at different temperatures far from the transition temperatures with the linear regression coefficients, and the values of (- $d\gamma_s^d/d\theta$) and $\gamma_s^d(0)$.

T(K)	Equation of $\gamma_s^d(\theta)$	R^2	- $d\gamma_s^d/d\theta$	$\gamma_s^d(0)$
303.15	$\gamma_s^d(\theta)$ = -38.63 θ + 116.32	0.994	38.63	116.32
313.15	$\gamma_s^d(\theta)$= -34.92 θ + 104.49	0.9779	34.92	104.49
323.15	$\gamma_s^d(\theta)$ = -33.44 θ + 93.92	0.985	33.44	93.92
328.15	$\gamma_s^d(\theta)$ = -23.85 θ + 87.36	0.9569	23.85	87.36
348.15	$\gamma_s^d(\theta)$= -23.40 θ + 76.95	0.9293	23.40	76.95
353.15	$\gamma_s^d(\theta)$ = -23.26 θ + 71.15	0.9865	23.26	71.15
363.15	$\gamma_s^d(\theta)$ = -22.75 θ + 61.70	0.9836	22.75	61.70
373.15	$\gamma_s^d(\theta)$ = -23.19 θ + 52.36	0.9658	23.19	52.36
413.15	$\gamma_s^d(\theta)$ = -13.59 θ + 31.82	0.9765	13.59	31.82
423.15	$\gamma_s^d(\theta)$ = -11.84 θ + 27.13	0.9751	11.84	27.13
463.15	$\gamma_s^d(\theta)$ = -8.69 θ + 16.72	0.9918	8.69	16.72
473.15	$\gamma_s^d(\theta)$ = -8.27 θ + 15.87	0.9904	8.27	15.87

Table 6 led to the following thermodynamic relations of (- $\frac{d\gamma_s^d}{d\theta}(T)$) and $\gamma_s^d(T,0)$ as a function of the temperature:

$$\begin{cases} -\frac{d\gamma_s^d}{d\theta}(T) = 8\times10^{-4}\,T^2 - 0.759\,T + 197.04;\ R^2 = 0.9453 \\ \gamma_s^d(T,0) = 2.8\times10^{-3}\,T^2 - 2.77\,T + 696.64;\ R^2 = 0.9972 \end{cases} \quad (3)$$

Relations 3 then gave a universal equation of the following form:

$$\gamma_s^d(T,\theta) = \frac{d\gamma_s^d}{d\theta}(T)\,\theta + \gamma_s^d(T,0) \quad (4)$$

Equation (4) is the general form of the dependence of the London dispersive surface energy of the composites PMMA/silica on the temperature and the recovery fraction θ. The expression of $\gamma_s^d(T,0)$ given in relation 3 gave the same equation as that obtained with the silica particles (for $\theta = 0$). The obtained linearity of γ_s^d as a function of θ is not realized with the temperature. Indeed, the second-degree equation of (- $\frac{d\gamma_s^d}{d\theta}(T)$) and $\gamma_s^d(T,0)$ versus the temperature gave a non-linearity dependence of $\gamma_s^d(T)$.

 doi:10.20944/preprints202404.1469.v1

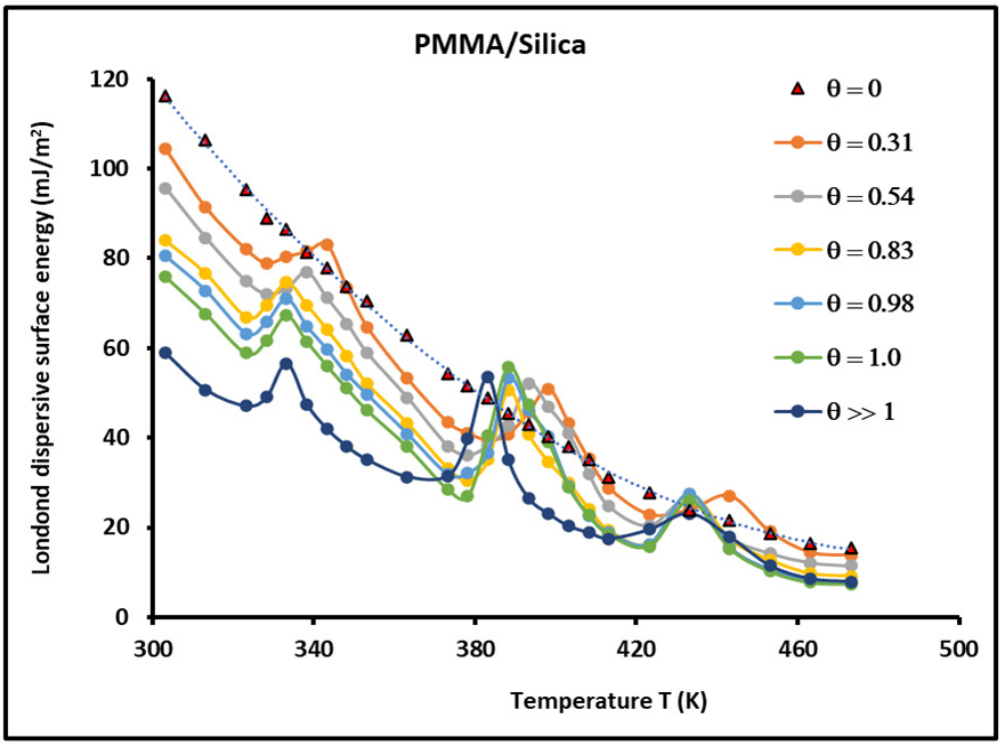

(a)

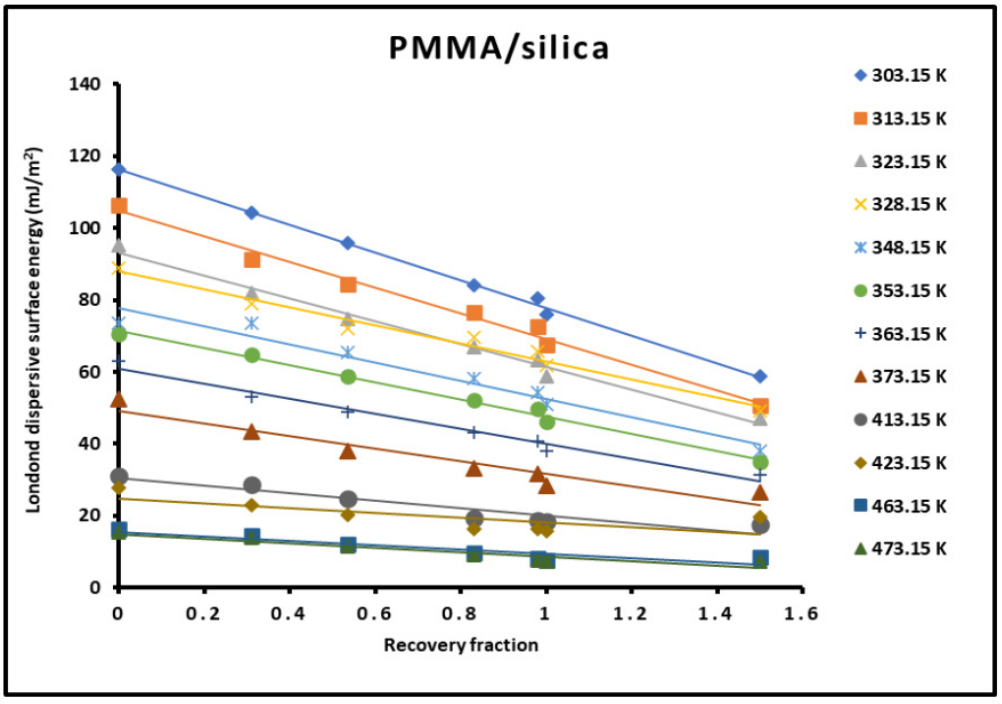

(b)

Figure 6. Variations of the London dispersive energy of silica and PMMA adsorbed on silica particles as a function of the temperature and the recovery fraction PMMA/Silica. (a) $\gamma_s^d(T)$, and (b) $\gamma_s^d(\theta)$.

 doi:10.20944/preprints202404.1469.v1

3.3. Lewis's Acid-Base Polar Surface Energies of PMMA/Silica

Van Oss et al. method [69] was used to determine the Lewis acid γ_s^+ and base γ_s^- surface energies of PMMA/silica knowing the Lewis acid γ_l^+ and base γ_l^- surface energies of the used solvents. Van Oss et al. used two monopolar solvents, namely, ethyl acetate (EA) and dichloromethane (DCM), usually characterized by:

$$\begin{cases} \gamma_{DCM}^+ = 5.2\ mJ/m^2\ , \gamma_{DCM}^- = 0 \\ \gamma_{EA}^+ = 0\ , \gamma_{EA}^- = 19.2\ mJ/m^2 \end{cases} \quad (5)$$

In previous studies [55,68], the polar free energy $\Delta G_a^{sp}(T)$ of the different composites PMMA/silica was determined as a function of the temperature with various recovery fractions. Knowing that $\Delta G_a^{sp}(T)$ can be expressed as follows:

$$\Delta G_a^{sp}(T) = 2\mathcal{N}a\left(\sqrt{\gamma_l^-\gamma_s^+} + \sqrt{\gamma_l^+\gamma_s^-}\right) \quad (6)$$

The Lewis acid and base surface energies of the various composites PMMA/silica were determined with the help of the following equations:

$$\begin{cases} \gamma_s^+ = \frac{\left[\Delta G_a^{sp}(T)\,(EA)\right]^2}{4\mathcal{N}^2[a(EA)]^2\gamma_{EA}^-} \\ \gamma_s^- = \frac{\left[\Delta G_a^{sp}(T)\,(DCM)\right]^2}{4\mathcal{N}^2[a(DCM)]^2\gamma_{DCM}^+} \end{cases} \quad (7)$$

and by using the values of the surface area of polar molecules obtained from the Hamieh thermal model. The obtained values of $\Delta G_a^{sp}(T)$ of EA and DCM adsorbed on the different solid surfaces were given in Tables S3 and S4. The polar (or acid-base) surface energy γ_s^{AB} and the total surface energy of different PMMA/silica composites were obtained from Eq. 8.

$$\begin{cases} \gamma_s^{AB} = 2\sqrt{\gamma_s^+\gamma_s^-} \\ \gamma_s^{tot.} = \gamma_s^d + \gamma_s^{AB} \end{cases} \quad (8)$$

The results were presented in Table S5 and Figure 7. All surface energy parameters of the various PMMA/silica varied as a function of the temperature as shown in Figure 7.

 doi:10.20944/preprints202404.1469.v1

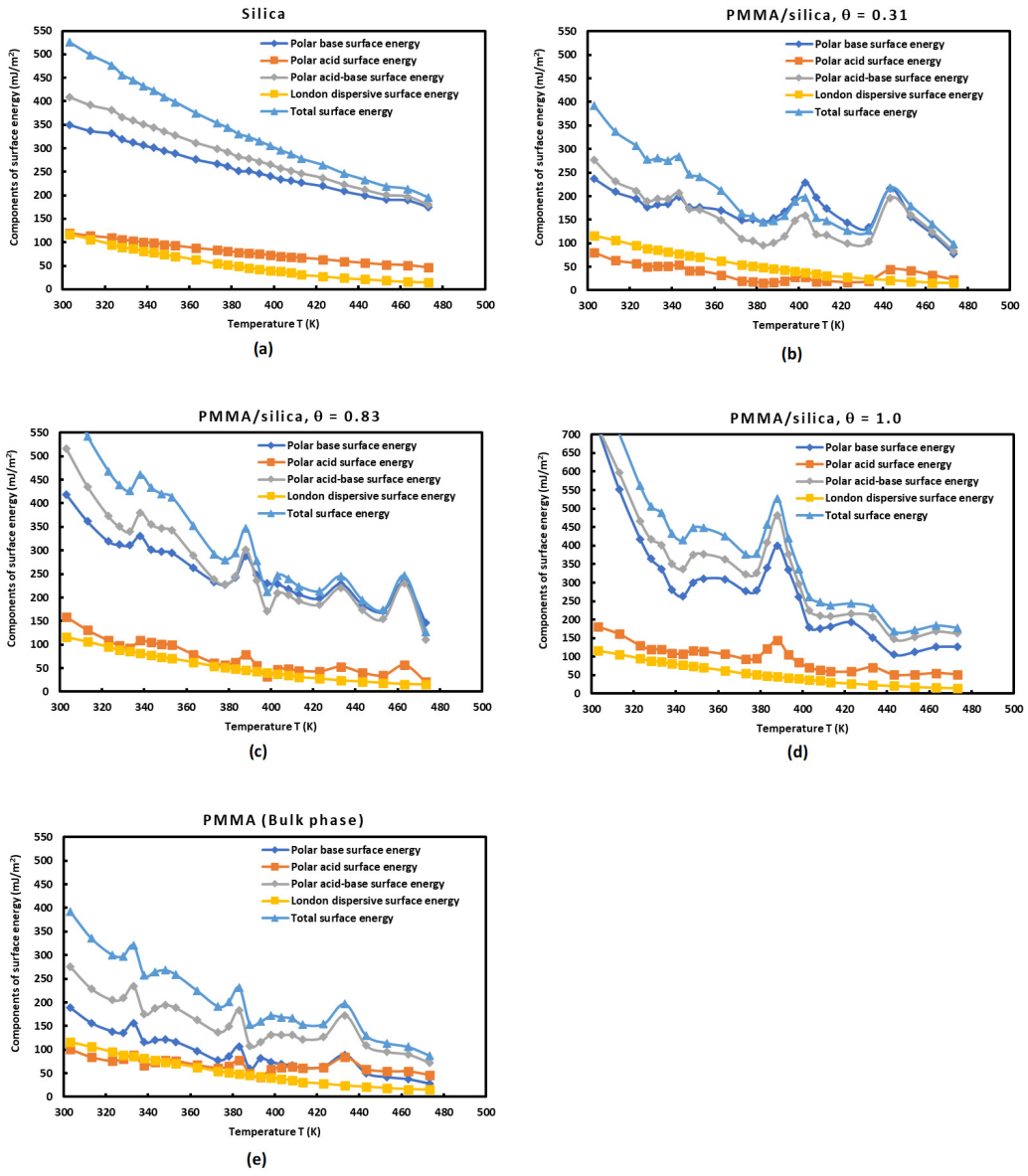

Figure 7. Variations of $\gamma_s^+(T)$, $\gamma_s^-(T)$, $\gamma_s^{AB}(T)$, $\gamma_s^{tot.}(T)$, and $\gamma_s^d(T)$ of silica particles and PMMA adsorbed on silica as a function of the temperature, at different recovery fractions. (a) $\theta = 0$ (*silica case*), (b) $\theta = 0.31$, (c) $\theta = 0.83$, (d) $\theta = 1.0$, and (e) $\theta \gg 1$ (*PMMA case*).

Several conclusions can be deduced:

- All curves of the acid-base polar surface energies decreased against the temperature, except at the transition temperature where higher values of these parameters were observed for the different recovery fractions.
- The acid polar surface energy of silica did not present any appreciated variation when the recovery fraction of PMMA increased. Globally, the acidity of silica particles is not very affected by the adsorbed amount of PMMA.
- An important change in the value of the base polar surface energy $\gamma_s^-(T)$ was observed when the recovery fraction of PMMA varied. It seems that a maximum of $\gamma_s^-(T)$ was obtained in the case of a monolayer ($\theta = 1.0$) of PMMA adsorbed on silica particles and the acid-base polar surface energy γ_s^{AB} was the highest in this later case. For this value of $\theta = 1.0$, a maximum of $\gamma_s^{tot.}(T)$ was also observed. In the case of monolayer of adsorption of PMMA on silica, it can be

 doi:10.20944/preprints202404.1469.v1

deduced that the polar surface energy was higher than those of silica and PMMA taken separately, and it approximately approached the summation of these two extreme cases of $\theta = 0$ $(Silica)$ and PMMA in bulk phase.

4. Conclusions

The adsorption of PMMA on silica particles at different recovery fractions was studied as a function of the temperature by using the inverse gas chromatography (IGC) at infinite dilution. The IGC technique gave the experimental values of $RTlnV_n$ of n-alkanes adsorbed on the different PMMA/silica composites. Several molecular models were used and compared to the recent Hamieh thermal model to determine the variations of the London dispersive surface energy of solid particles as a function of the temperature and the recovery fraction of PMMA adsorbed on silica. The determination of $\gamma_s^d(T)$ of silica particles by using the thermal model showed parabolic variations with an excellent regression coefficient approaching 1.000. The other molecular models gave the same type of variations of $\gamma_s^d(T)$, but with important deviation from the accurate thermal model taking into account the effect of the temperature on the surface area of organic molecules. The curves of $\gamma_s^d(T)$ of the PMMA/silica systems confirmed the presence of three maxima characterizing the three transition temperatures of the beta-relaxation, the glass transition and the liquid-liquid transition. An important effect of the recovery fraction of PMMA on the values of the transition temperatures was highlighted in this study.

A universal equation of $\gamma_s^d(T,\theta)$ of the various PMMA/silica composites was given as a function of the two variables, the temperature T, and the recovery fraction θ. The determination of the couple (T,θ) led to obtain the value of γ_s^d and the full thermodynamic determination of the system PMMA/silica

The Lewis acid γ_s^+ and base γ_s^- polar surface energies of PMMA/silica composites were determined by using the thermal model as a function of the temperature and the recovery fraction. the polar acid–base surface energy γ_s^{AB} and the total surface energy of the different composites were then deduced. It was showed that γ_s^+ of silica was not so much affected by the adsorption of PMMA on silica, whereas, γ_s^- presented large variations when the recovery fraction varied. A maximum of basic and total polar surface energies was reached in the case of monolayer of PMMA. The total polar surface energy of PMMA/silica for a monolayer ($\theta = 1.0$) was proved to be approximately equivalent, out of the transition temperatures, to the summation of those obtained with silica and PMMA solid surfaces.

Supplementary Materials: The following supporting information can be downloaded at www.mdpi.com/xxx/s1: Table S1. Values of $RTlnVn$ (kJ/mol) of n-alkanes adsorbed on silica particles as a function of the temperature.Table S2. Values of parameter $2\mathcal{N}a\left(\gamma_l^d\right)^{1/2}$ $(m^2 \times mJ^{1/2})$ of n-alkanes adsorbed on solid particles as a function of the temperature. Table S3. Variations of $\Delta G_a^{sp}(T)$ (kJ/mol) of dichloromethane adsorbed on silica particles and PMMA/silica as a function of the temperature, at different recovery fractions. $\theta = 0$ $(silica\ case)$, $\theta = 0.31$, $\theta = 0.83$, $\theta = 1.0$, and $\theta \gg 1$ $(PMMA\ case)$.Table S4. Variations of $\Delta G_a^{sp}(T)$ (kJ/mol) of ethyl acetate adsorbed on silica particles and PMMA/silica as a function of the temperature, at different recovery fractions. $\theta = 0$ $(silica\ case)$, $\theta = 0.31$, $\theta = 0.83$, $\theta = 1.0$, and $\theta \gg 1$ $(PMMA\ case)$.Table S5. Values of $\gamma_s^+(T)$, $\gamma_s^-(T)$, $\gamma_s^{AB}(T)$, $\gamma_s^d(T)$, and $\gamma_s^{tot.}(T)$ of silica particles and PMMA adsorbed on silica as a function of the temperature, at different recovery fractions: $\theta = 0$ $(silica\ case)$, $\theta = 0.31$, $\theta = 0.83$, $\theta = 1.0$, and $\theta \gg 1$ $(PMMA\ case)$.

Funding: This research did not receive any specific funding.

Institutional Review Board Statement: Not applicable.

Informed Consent Statement: Not applicable.

Data Availability Statement: There are no additional data.

Conflicts of Interest: The author declares no conflicts of interest.

References

1. Papadopoulou, S.K.; Panayiotou, C. Assessment of the thermodynamic properties of poly(2,2,2-trifluoroethyl methacrylate) by inverse gas chromatography, *J. Chromatogr. A*, **2014**, 1324, 207– 214.
2. Voelkel, A.; Strzemiecka, B.; Adamska, K.; Milczewska, K.; *J. Chromatogr.*, **2009**, *A* 1216, 1551.
3. Al-Saigh, Z.Y.; Munk, P. *Macromolecules*, **1984**, 17, 803.
4. Dritsas, G.S.; Karatasos, K.; Panayiotou, C. *J. Chromatogr. A*, **2009**, 1216, 8979.
5. Papadopoulou, S.K. ; Karapanagiotis, I. ; Zuburtikudis, I. ; Panayiotou, C. *J. Polym. Sci. B*: *Polym. Phys*. **2010**, 48, 1826.
6. Papadopoulou, S.K. ; Panayiotou, C. *J. Chromatogr. A*, **2012**, 1229, 230.
7. J.F. Gamble, J.F.; Dave, R.N.; Kiang, S.; Leane, M.M.; Tobyn, M.; Wang, S.S.Y. *Int. J. Pharm*. **2013**, 445, 39.
8. Kołodziejek, J.; Voelkel, A.; Heberger, K.; *J. Pharm. Sci*., **2013**, 102, 1524.
9. Heydar, K.; Nazifi, M.; Sharifi, A.; Mirzaei, M.; Gharavi, H.; Ahmadi, S. *Chromatographia*, **2013**, 76, 165.
10. Doman' ska, U.; Lukoshko, E.V.; *J. Chem. Therm*., **2013**, 66, 144.
11. B. Yoo, W. Afzal, J.M. Prausnitz, Ind. Eng. Chem. Res. 51 (2012) 9913.
12. P. Lazar, P. et al., *J. Am. Chem. Soc*., **2013**, 135, 6372.
13. Belgacem, M.N.; Czeremuszkin, G.; Sapieha, S.; Gandini, A. *Cellulose*, **1995**, 2, 145.
14. Papadopoulou, S.K. et al., *Colloids Surf. A*, **2011**, 387, 71.
15. Ryan, H. M.; Douglas, J. G.; Rupert W. Inverse Gas Chromatography for Determining the Dispersive Surface Free Energy and Acid–Base Interactions of Sheet Molding Compound-Part II 14 Ligno-Cellulosic Fiber Types for Possible Composite Reinforcement, *Journal of Applied Polymer Science*, **2008**, 110, 3880–3888.
16. Jacob, P. N.; Berg, J. C. *Langmuir*, **1994**, 10, 3086.
17. Carvalho, M. G.; Santos, J. M. R. C. A.; Martins, A. A.; Figueiredo, M. M. *Cellulose*, **2005**, 12, 371.
18. Chtourou, H.; Riedl, B.; Kokta, B. V. *J Adhesion Sci Tech*, **1995**, 9, 551.
19. Dorris, G. M.; Gray, D. G. J Colloid Interface Sci., **1980**, 77, 353. Riedl, B.; Matuana, L. M. *Encycl Surface Colloid Sci*, **2002**, 2842.
20. Donnet, J. B.; Park, S. J.; Balard, H.; *Chromatographia*, **1991**, 31(9/10), 434.
21. Gutmann, V. The Donor Acceptor Approach to Molecular Interactions; Plenum: New York, 1978; Chapter 2.
22. John F. Gamble, Rajesh N. Dave, San Kiang, Michael M. Leane, Mike Tobyn, Steve S.Y. Wang, Investigating the applicability of inverse gas chromatography to binary powdered systems: An application of surface heterogeneity profiles to understanding preferential probe-surface interactions, *International Journal of Pharmaceutics*, **2013**, 445, 39– 46
23. Balard, H. ; Maafa, D. ; Santini, A. ; Donnet, J.B. Study by inverse gas chromatography of the surface properties of milled graphites. *J. Chromatogr. A*, **2008** 1198–1199, 173–180.
24. Bogillo, V.I.; Shkilev, V.P.; Voelkel, A. Determination of surface free energy components for heterogeneous solids by means of inverse gas chromatography at finite concentrations. *J. Mater. Chem.* **1998**, 8, 1953–1961.
25. Das, S.C.; Zhou, Q.; Morton, D.A.V.; Larson, I.; Stewart, P.J. Use of surface energy distributions by inverse gas chromatography to understand mechanofusion processing and functionality of lactose coated with magnesium stearate. *Eur. J. Pharm. Sci*., **2011**. 43, 325–333.
26. Das, S.C.; Stewart, P.J. Characterising surface energy of pharmaceutical powders by inverse gas chromatography at finite dilution. *J. Pharm. Pharmacol*., **2012**, 64, 1337–1348.
27. Dorris, G.M.; Gray, D.G. Adsorption of n-alkanes at zero surface coverage on cellulose paper and wood fibres. *J. Colloid Interface Sci*., **1980**, 77, 353–362.
28. Dong, S. ; Brendlé, M.; Donnet, J.B. Study of solid surface polarity by inverse gas chromatography at infinite dilution. *Chromatographia*, **1989**, 28, 469–472.
29. Feeley, J.C.; York, P.; Sumby, B.S.; Dicks, H. Determination of surface properties and flow characteristics of salbutamol sulphate, before and after micronisation. *Int. J. Pharm*., **1998**, 172, 89–96.
30. Gamble, J.F.; Leane, M.; Olusanmi, D.; Tobyn, M.; Supuk, E.; Khoo, J.; Naderi, M. Surface energy analysis as a tool to probe the surface energy characteristics of micronized materials – a comparison with inverse gas chromatography, *Int. J. Pharm.*, **2012**, 422, 238–244.
31. Newell, H.E.; Buckton, G.; Butler, D.A.; Thielmann, F.; Williams, D.R. The use of inverse gas chromatography to measure the surface energy of crystalline, amorphous, and recently milled lactose. *Pharm. Res*., **2001**, 18, 662–666.
32. Newell, H.E.; Buckton, G. Inverse gas chromatography: investigating whether the technique preferentially probes high energy sites for mixtures of crystalline and amorphous lactose. *Pharm. Res.*, **2004**, 21, 1440–1444.
33. Kołodziejek, J.; Głowka, E.; Hyla, K.; Voelkel, A.; Lulek, J.; Milczewska, K. Relationship between surface properties determined by inverse gas chromatography and ibuprofen release from hybrid materials based on fumed silica, *International Journal of Pharmaceutics*, **2013**, 441, 441– 448.
34. Ho, R.; Wilson, D.A.; Heng, J.Y.Y. Crystal habits and the variation in surface energy heterogeneity. *Cryst. Growth Des*., **2009**, 9 (11), 4907–4911.

35. Ho, R.; Hinder, S.J.; Watts, J.F.; Dilworth, S.E.; Williams, D.R.; Heng, J.Y.Y. Determination of surface heterogeneity of D-mannitol by sessile drop contact angle and finite concentration inverse gas chromatography. *Int. J. Pharm*., **2010**, 387 (1), 79–86.
36. Ho, R., Naderi, M.; Heng, J.Y.Y.; Williams, D.R.; Thielmann, F.; Bouza, P.; Keith, A.R.; Thiele, G.; Burnett, D.J. Effect of milling on particle shape and surface energy heterogeneity of needle-shaped crystals. *Pharm. Res*., **2012**, 29, 2806–2816.
37. Sesigur, F.; Sakar, D.; Yazici, O.; Cakar, F.; Cankurtaran, O.; Karaman, F. Dispersive Surface Energy and Acid-Base Parameters of Tosylate Functionalized Poly(ethylene glycol) via Inverse Gas Chromatography, *Journal of Chemistry*, **2014**, 2014, 1-7.
38. Calvet, R.; Del Confetto, S.; Balard, H.; Brendlé, E.; Donnet, J.B. Study of the interaction polybutadiene/fillers using inverse gas chromatography, *Journal of Chromatography A*, **2012**, 1253, 164– 170.
39. Papadopoulou, S.K.; Dritsas, G.; Karapanagiotis, I.; Zuburtikudis, I.; Panayiotou, C. Surface characterization of poly(2,2,3,3,3-pentafluoropropyl methacrylate) by inverse gas chromatography and contact angle measurements, *European Polymer Journal*, **2010**, 46, 202–208.
40. Dritsas, G.S.; Karatasos, K.; Panayiotou, C. Investigation of thermodynamic properties of hyperbranched poly(ester amide) by inverse gas chromatography. *J Polym Sci Polym Phys*, **2008**, 46(20) 2166–2172.
41. Hamieh, T. Study of the temperature effect on the surface area of model organic molecules, the dispersive surface energy and the surface properties of solids by inverse gas chromatography. *J. Chromatogr. A* **2020**, *1627*, 461372.
42. Hamieh, T.; Ahmad, A.A.; Roques-Carmes, T.; Toufaily, J. New approach to determine the surface and interface thermodynamic properties of H-β-zeolite/rhodium catalysts by inverse gas chromatography at infinite dilution. *Sci. Rep.* **2020**, *10*, 20894.
43. Hamieh, T. New methodology to study the dispersive component of the surface energy and acid–base properties of silica particles by inverse gas chromatography at infinite dilution. *J. Chromatogr. Sci.* **2022**, *60*, 126–142. https://doi.org/10.1093/chromsci/bmab066.
44. Papirer, E.; Brendlé, E.; Ozil, F.; Balard, H. Comparison of the surface properties of graphite, carbon black and fullerene samples, measured by inverse gas chromatography. *Carbon* **1999**, *37*, 1265–1274. https://doi.org/10.1016/S0008-6223(98)00323-6.
45. Chung, D.L. *Carbon Fiber Composites*; Butterworth-Heinemann: Boston, MA, USA, 1994; pp. 3–65.
46. Donnet, J.B.; Bansal, R.C. *Carbon Fibers*, 2nd ed.; Marcel Dekker: New York, NY, USA, 1990; pp. 1–145.
47. Friedlander, H.N.; Peebles, L.H., Jr.; Brandrup, J.; Kirby, J.R. On the chromophore of polyacrylonitrile. VI. Mechanism of color formation in polyacrylonitrile. *Macromolecules* **1968**, *1*, 79–86. https://doi.org/10.1021/ma60001a014.
48. Huang, X. Fabrication and Properties of Carbon Fibers. *Materials* **2009**, *2*, 2369–2403. https://doi.org/10.3390/ma2042369.
49. Qiao, Z.; Ding, C. Recent progress in carbon fibers for boosting electrocatalytic energy conversion. *Ionics* **2022**, *28*, 5259–5273. https://doi.org/10.1007/s11581-022-04664-7.
50. Hamieh, T. Surface acid-base properties of carbon fibres. *Adv. Powder Technol*. **1997**, *8*, 279–289.
51. Le Vu, H.; Nguyen, S.H.; Dang, K.Q.; Pham, C.V.; Le, H.T. The Effect of Oxidation Temperature on Activating Commercial Viscose Rayon-Based Carbon Fibers to Make the Activated Carbon Fibers (ACFs). *Mater. Sci. Forum* **2020**, *985*, 171–176. https://doi.org/10.4028/www.scientific.net/MSF.985.171.
52. Liu, Y.; Gu, Y.; Wang, S.; Li, M. Optimization for testing conditions of inverse gas chromatography and surface energies of various carbon fiber bundles. *Carbon Lett.* **2023**, *33*, 909–920. https://doi.org/10.1007/s42823-023-00472-9.
53. Pal, A.; Kondor, A.; Mitra, S.; Thua, K.; Harish, S.; Saha, B.B. On surface energy and acid–base properties of highly porous parent and surface treated activated carbons using inverse gas chromatography. *J. Ind. Eng. Chem.* **2019**, *69*, 432–443. https://doi.org/10.1016/j.jiec.2018.09.046.
54. Hamieh, T. New Physicochemical Methodology for the Determination of the Surface Thermodynamic Properties of Solid Particles. *AppliedChem* **2023**, *3*, 229–255; https://doi.org/10.3390/appliedchem3020015.
55. Hamieh, T.; Schultz, J. New approach to characterise physicochemical properties of solid substrates by inverse gas chromatography at infinite dilution. I. Some new methods to determine the surface areas of some molecules adsorbed on solid surfaces. *J. Chromatogr. A* **2002**, *969*, 17–47. https://doi.org/10.1016/S0021-9673(02)00368-0.
56. Sawyer, D.T.; Brookman, D.J. Thermodynamically based gas chromatographic retention index for organic molecules using salt-modified aluminas and porous silica beads. *Anal. Chem*. **1968**, *40*, 1847–1850. https://doi.org/10.1021/ac60268a015.
57. Saint-Flour, C.; Papirer, E. Gas-solid chromatography. A method of measuring surface free energy characteristics of short carbon fibers. 1. Through adsorption isotherms. *Ind. Eng. Chem. Prod. Res. Dev*. **1982**, *21*, 337–341. https://doi.org/10.1021/i300006a029.

 doi:10.20944/preprints202404.1469.v1

58. Saint-Flour, C.; Papirer, E. Gas-solid chromatography: Method of measuring surface free energy characteristics of short fibers. 2. Through retention volumes measured near zero surface coverage. *Ind. Eng. Chem. Prod. Res. Dev*. **1982**, *21*, 666–669. https://doi.org/10.1021/i300008a031.
59. Donnet, J.-B.; Park, S.; Balard, H. Evaluation of specific interactions of solid surfaces by inverse gas chromatography. *Chromatographia* **1991**, *31*, 434–440.
60. Brendlé, E.; Papirer, E. A new topological index for molecular probes used in inverse gas chromatography for the surface nanorugosity evaluation, 2. Application for the Evaluation of the Solid Surface Specific Interaction Potential. *J. Colloid Interface Sci*. **1997**, *194*, 217–224.
61. Brendlé, E.; Papirer, E. A new topological index for molecular probes used in inverse gas chromatography for the surface nanorugosity evaluation, 1. Method of Evaluation. *J. Colloid Interface Sci*. **1997**, *194*, 207–216.
62. Hamieh, T. Some Irregularities in the Evaluation of Surface Parameters of Solid Materials by Inverse Gas Chromatography, *Langmuir,* **2023,** *39, 17059-17070,* https://doi.org/10.1021/acs.langmuir.3c01649.
63. Gutmann, V. The Donor-acceptor Approach to Molecular Interactions; Plenum: New York, NY, USA, 1978.
64. Hamieh, T. The Effect of Temperature on the Surface Energetic Properties of Carbon Fibers Using Inverse Gas Chromatography, *Crystals,* **2024**, *14*(1), 28; https://doi.org/10.3390/cryst14010028.
65. Hamieh, T. New Progress on London Dispersive Energy, Polar Surface Interactions, and Lewis's Acid–Base Properties of Solid Surfaces, Molecules, **2024**, 29 (5), 949, https://doi.org/10.3390/molecules29050949
66. Hamieh, T. London Dispersive and Lewis Acid-Base Surface Energy of 2D Single-Crystalline and Polycrystalline Covalent Organic Frameworks, *Crystals,* **2024**, *14*(2), 148; https://doi.org/10.3390/cryst14020148
67. Hamieh, T. Inverse Gas Chromatography to Characterize the Surface Properties of Solid Materials, *Chem. Mater.* 2024, 36, 5, 2231-2244, https://doi.org/10.1021/acs.chemmater.3c03091
68. T Hamieh, Temperature Dependence of the Polar and Lewis Acid–Base Properties of Poly Methyl Methacrylate Adsorbed on Silica via Inverse Gas Chromatography, Molecules 29 (8), 1688, https://doi.org/10.3390/molecules29081688
69. Van Oss, C.J.; Good, R.J.; Chaudhury, M.K. Additive and nonadditive surface tension components and the interpretation of contact angles. *Langmuir* **1988**, *4*, 884. https://doi.org/10.1021/la00082a018.